

# Shock-Initiated Buckling of Carbon/Epoxy Composite Tubes at Sub-Critical Pressures

M. Pinto<sup>1</sup> · A. Shukla<sup>1</sup>

Received: 4 February 2015 / Accepted: 20 April 2015 / Published online: 29 April 2015  
© Society for Experimental Mechanics 2015

**Abstract** A comprehensive investigation on the implosion of composite cylinders subjected to a nearby explosion is performed. Experiments are conducted in a large pressure vessel, designed to provide constant hydrostatic pressure throughout the event. Carbon fiber/epoxy filament-wound tubes are studied with constant hydrostatic pressure and varying charge standoff distances to determine the effect of the explosive loading on the mechanisms of collapse. 3-D Digital Image Correlation (DIC) is used to capture the full-field displacements and velocities during the implosion event, and to characterize the initial dynamic response of the tube. Dynamic pressure transducers measure the shock waves generated by the explosive and also the pressure pulse generated by the collapse. Results show that different magnitudes of explosive loading produce drastic differences in the way implosions are initiated, and in the extent of damage to the structure. Experiments with strong explosive loading show immediate collapse of the tube upon the arrival of shock wave. Relatively smaller explosive loading result in collapses due to the additional bubble pulse loading, or after accumulating damage for extended periods of time.

**Keywords** Composite tubes · Implosion · Digital image correlation · High-speed photography · Underwater explosive loading (UNDEX)

## Introduction

In recent decades, there has been increased interest in using composites for naval and marine applications. As compared to metals, composite materials have reduced weight, improved corrosion resistance, and greater operating depths for submerged environments. However, widespread adaptation of composite materials is hindered by a lack of complete understanding and simple design rules, especially for extreme loading conditions [1]. One such condition in undersea applications is that of implosion. Implosion is the rapid collapse of a sealed, thin-walled structure subjected to external pressure. When the applied external pressure reaches a critical value, the structure becomes unstable and its walls buckle inward, causing the tube to collapse completely. An implosion caused by quasi-static pressurization to this critical pressure is known as a natural implosion. However, implosions can also be initiated at sub-critical pressures with an underwater explosive (UNDEX) loading. If a structure experiences a high magnitude shock –wave loading such as that generated by a near-field UNDEX, it may collapse at a relatively low hydrostatic pressure [2]. This work focuses on addressing this extreme condition for composite materials.

Some experimental work has been performed on the implosion of composite tubes, however these studies are limited to hydrostatic implosion and typically concerned only with evaluating collapse pressure [3–6]. Most recently, the hydrostatic implosion of carbon fiber and glass fiber reinforced tubes was studied experimentally by the authors using Digital Image Correlation to relate collapse mechanics to the changes in local pressure fields [7, 8]. Some numerical studies have been performed on implosions initiated by explosive loading in recent years. Pegg studied the mechanics of explosive initiated implosions of homogenous materials and how the qualities of the impulse affect the instability [9]. Tanov et al examined the effect of static preloading on the impulse

---

✉ A. Shukla  
shuklaa@egr.uri.edu

<sup>1</sup> Dynamics Photomechanics Laboratory, Department of Mechanical, Industrial and Systems Engineering, University of Rhode Island, Kingston, RI 02881, USA

driven implosion of composite tubes using finite elements [10]. Krueger also used finite element models to study explosive initiated implosion of metallic tubes with varying impulse strengths [11]. Fatt et. al developed stability diagrams for composite cylinders under shock loading using Mathieu equations [12]. A few experimental studies also exist on the response of closed cylinders to underwater explosions. Both Brett and Yiannakopolous [13] and Hung et. al [14] independently evaluated the dynamic response of metallic cylinders subjected to a nearby explosive. In addition, Ikeda performed experiments on the explosive initiated implosion of metallic tubes with varying loading, to define the conditions for a collapse to occur [15]. Finally, Arora et. al performed experiments on the effects of air and underwater blast loading on composite panels and tube structures [16]. However, no experimental work exists on explosive initiated implosions of composite materials, and what numerical work does exist does not account for material damage.

This study looks to address this gap in understanding by using high-speed photography coupled with Digital Image Correlation to explore the implosion of composite tubes subjected to shock waves of different strengths. Experiments also focus on the interaction of the bubble pulse with the structure, and its effect on the implosion process. Depending on the stand-off distance of the charge, the tube may implode due to different features of the explosive pressure history. This will also change the degree of damage incurred in the structure, as well as the effect of the collapse on the local pressure field.

## Experimental Details

The impodable volumes in this study are carbon/epoxy filament wound composite tubes, consisting of seven layers of

unidirectional carbon fabric reinforcement arranged in a  $[\pm 15/0/\pm 45/\pm 15]$  layout with a 60.3mm inner diameter and 381mm unsupported length. These cylinders are manufactured by Rock West Composites (West Jordan, UT) with a nominal wall thickness of 1.63mm. The dimensions are selected as to provide specimens with a relatively low expected collapse pressure, and a high radius-to-thickness ratio so that thin-wall assumptions may be utilized.

The explosives used are RP-85 exploding-bridgewire (EBW) detonators manufactured by Teledyne RISI, Inc. (Tracy, CA). The output explosive material in these detonators is 1031mg of RDX (cyclotrimethylenetrinitramine), initiated by 80mg of PETN (pentaerythritol tetranitrate), the combination of which is equivalent to 1778mg of TNT.

All experiments are conducted in a 2.1m diameter spherical pressure vessel, able to provide constant hydrostatic pressure throughout the collapse event (see Fig. 1). Several acrylic windows mounted about the midspan of the pressure vessel allow the specimens to be viewed by cameras and adequately lit by two high intensity light sources.

The specimen is sealed using two aluminum end caps then suspended horizontally in the center of the pressure vessel using steel cables secured to the inner walls of the vessel. To measure the incident shock wave loading and the changes in local pressure during the collapse event, high pressure blast transducers (PCB 138A05, PCB Piezotronics, Inc., Depew, NY) are mounted at different locations about the specimen. Two sensors are located at the midspan of the specimen, and four sensors are located at axial offsets of 127mm from the midspan. All sensors are mounted such that the distance between the sensing element and the outer surface of the tube is nominally 55mm. The amplified outputs of these sensors are recorded at a sampling rate of 2 MHz. The explosive charge is secured directly behind the specimen at a given standoff

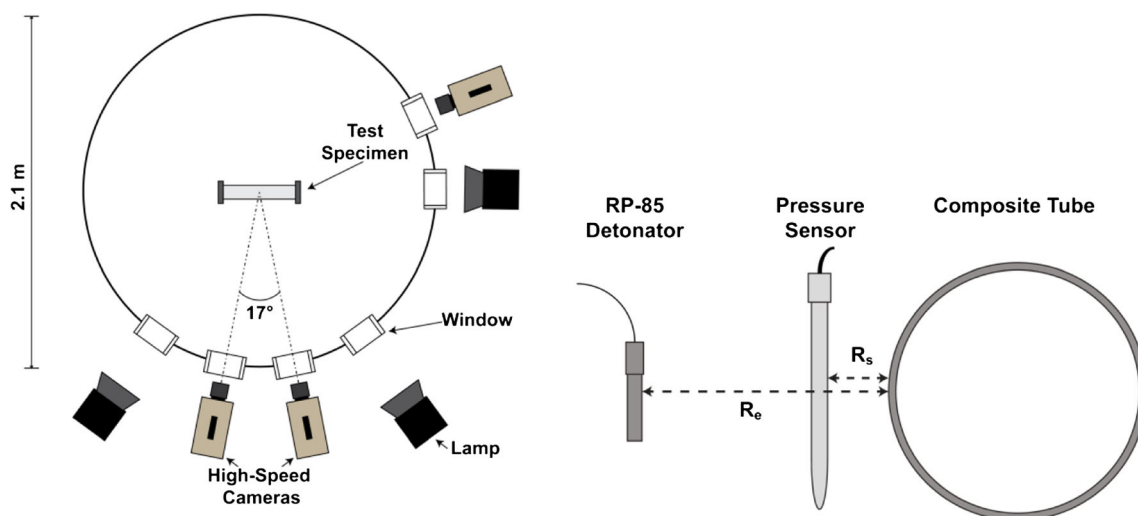


**Fig. 1** Diagram of experimental setup (*left*) and image of charge and sensor positioning (*right*), with the standoff distances of the detonator ( $R_e$ ) and the sensor ( $R_s$ ) clearly defined

distance so as not to interfere with photography, and is aligned with the center of the implodable volume (see Fig. 1).

The vessel is then flooded with filtered water, leaving a small air pocket. Once the vessel is filled, nitrogen gas is introduced into the air pocket to pressurize the enclosed water to the desired hydrostatic pressure. The pressure is increased slowly at a rate of 0.083 MPa/min to the chosen value. For this study, all experiments used a hydrostatic pre-pressure of 80% of the critical collapse pressure of the specimen. Following pressurization, the explosive is detonated using a high voltage firing unit which simultaneously triggers all data acquisition systems to record the event.

Prior to experiments, a random, high-contrast speckle pattern is applied by hand to a region spanning the entire length of the specimen and approximately half of the circumference using flat black and white paint. Features of the pattern were made sufficiently large as to occupy at least 3x3 pixels in the recorded images for optimal DIC measurements. Two high-speed cameras (Photron SA1, Photron USA, Inc.) positioned at a stereo angle of 17°, are used to capture images of the patterned region of the specimen at a frame rate of 75,000 frames/second. The stereo images are analyzed using a commercially available DIC software, VIC3D 2012 (Correlated Solutions, Inc., Columbia, SC) to measure full-field displacements across the viewable surface of the specimen. 3-D Digital image correlation (DIC) is a well known non-contact optical technique to determine real-time, full-field displacements across the viewable surface of a specimen [17]. This technique is calibrated for underwater experiments based on previous work [18] for confidence in the accuracy of measured displacements and velocities. Using the referenced calibration method, in-plane and out-of-plane displacements may be determined within 1.2% and 2.5% error, respectively. A third high speed camera is used to observe the charge itself to track the growth and collapse of the gas bubble, and is set to record at 40,000 fps.

## Results

### Natural Implosion Experiments

Prior to explosive initiated series, several natural implosion experiments are performed on the tubes to be studied to determine the critical collapse pressure and to characterize the collapse and local pressure field in the case of a natural implosion. These experiments are performed in the same manner as recently published work by this group [7, 8]. The critical collapse pressure of these tubes was found to be 0.90MPa. The pressure profile is plotted in Fig. 2, along with the displacement and velocity of the center point of the tube. High-speed photographs of the tube at different times during the collapse are included in Fig. 3. In these plots,  $t=0$ ms represents the instant that opposing walls of the tube make contact with each other.

It can be seen that the implosion of these tubes is quite similar to that of metallic tubes [19, 20] as well as other composite tubes studied by this group [7, 8]. Starting at  $t=-4.7$ ms, the walls of the tube begin to accelerate inward as observed in the displacement and velocity traces. As the walls accelerate, the local pressure decays to a minimum just prior to  $t=0$ ms. At  $t=0$ ms, opposing walls contact each other, resulting in the rapid deceleration of the walls. This imposes a large change in momentum onto the surrounding fluid, resulting in the high magnitude ( $\sim 1.30$ MPa) pressure pulse seen shortly thereafter. Following wall contact, the buckle propagates axially through the length of the tube until the entire tube is flattened. From the high-speed images in Fig. 3, it is seen that the tube remains free of visible damage until just before the time of wall contact. At  $t=-0.013$ ms, extreme bending at the two lobes of the buckling shape cause through-thickness cracking parallel to the length axis of the tube. Post-mortem analysis shows that damage is mainly restricted to these two longitudinal cracks, which propagate through nearly the entire length of the specimen.

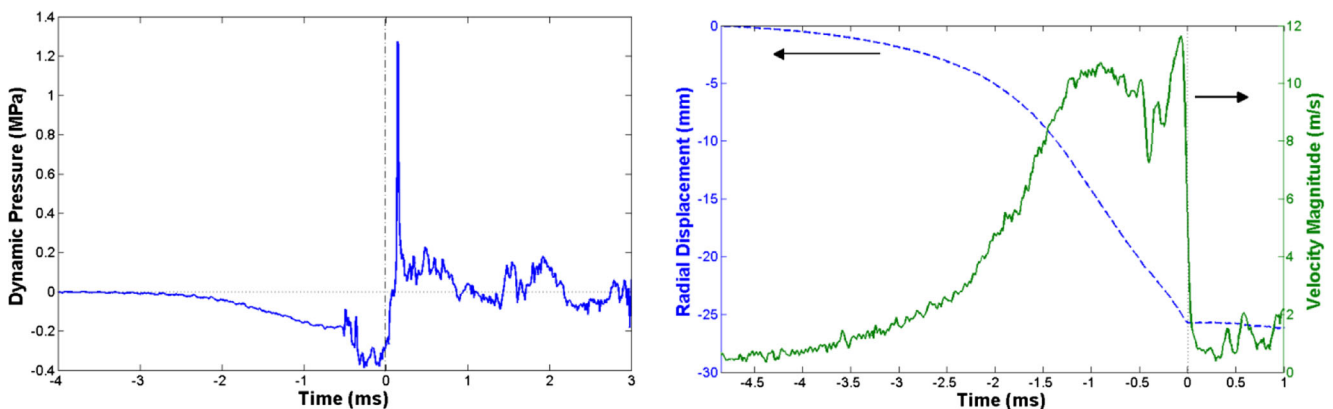


**Fig. 2** For a natural implosion, pressure history about the midspan of the specimen (*left*) and radial displacement and velocity curves measured at the center of the specimen (*right*)

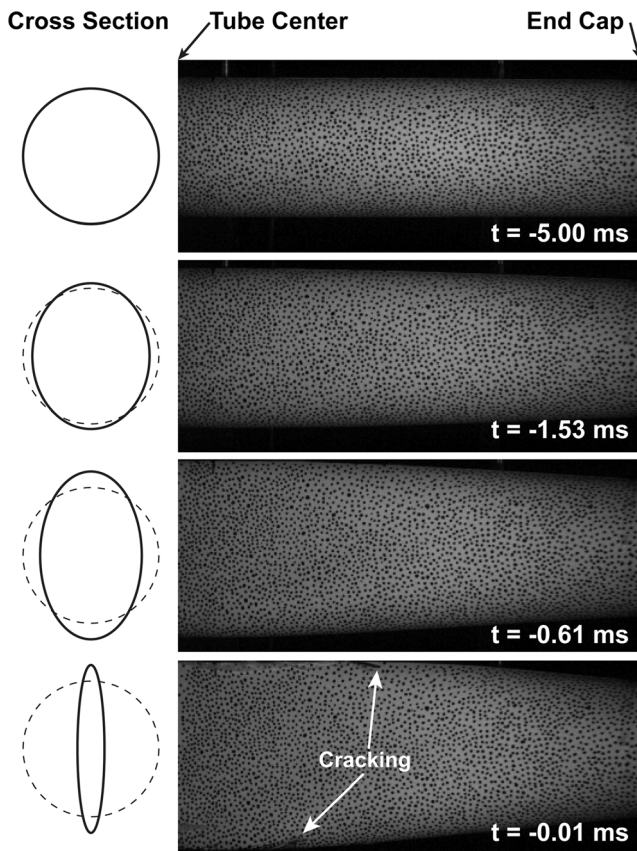


**Fig. 3** High-speed images taken at various times during the natural implosion experiments. Illustrations of the tube cross-section are to the left of the respective image. The tube is seen to buckle without visible damage until 0.013 ms prior to wall contact

The experiments described above were used to design the explosive initiated implosion series, which is summarized in Table 1. For all experiments in this series, the hydrostatic pre-pressure is kept constant at 80% of the critical collapse pressure, or 0.71 MPa. Three different explosive standoff distances are used, 102 mm, 203 mm, and 305 mm. These standoffs are chosen to impart different magnitude shock waves to the specimens while not allowing the gas bubble to interact with the tube. At least 2 experiments are performed for each case, to demonstrate repeatability of results. For each case, the tube did implode, but the time at which the implosion initiated after the explosion is different for each standoff distance. This

**Table 1** Summary of explosive-initiated implosion experiments

Case	Hydrostatic pressure (MPa)	Explosive standoff (mm)	Maximum predicted incident pressure (MPa)	Time before implosion (ms)
1	0.71	102	45.9	0.93
2	0.71	203	20.2	6.83
3	0.71	305	12.4	15.22

implies that for different standoff distances, different features of the explosive pressure history trigger the collapse, and therefore the mechanics at play in each case is unique.

### Interaction of Shock Wave with Specimen

One important thing to understand when studying the problem of an explosive initiated implosion is how the pressure wave interacts with the specimen. It is well known that the initial shock wave released from an UNDEX may be treated as an acoustic pressure pulse that travels at roughly sound speed once fully developed [21]. This allows the use of acoustic theory in analyzing the behavior of the wave. As an example, the pressure recorded at two different locations about the midspan of the tube for the case of a 305 mm explosive standoff is plotted in Fig. 4. Comparing pressure histories recorded at a sensor between the charge and the specimen (Sensor 1 in Fig. 4) and at a sensor above the specimen (Sensor 2 in Fig. 4), an interesting phenomenon is observed. In all experiments, it is seen that sensors located between the charge and the specimen record the initial high magnitude shock followed by a negative pressure spike of appreciable magnitude less than 0.1 ms later. In contrast, sensors located above the tube record only the initial pulse, followed by a smaller pressure “tail” that is typical of shock waves.

Because the delay between the initial spike and the negative pulse is slightly greater than the acoustic travel time for twice the distance from the sensor to the specimen ( $2 \times 70$  mm), the interface between the fluid and the specimen was further studied. When an acoustic wave encounters a boundary between two different materials, part of the wave will be transmitted into the second material while part will be reflected back into the first material. The reflected and transmitted

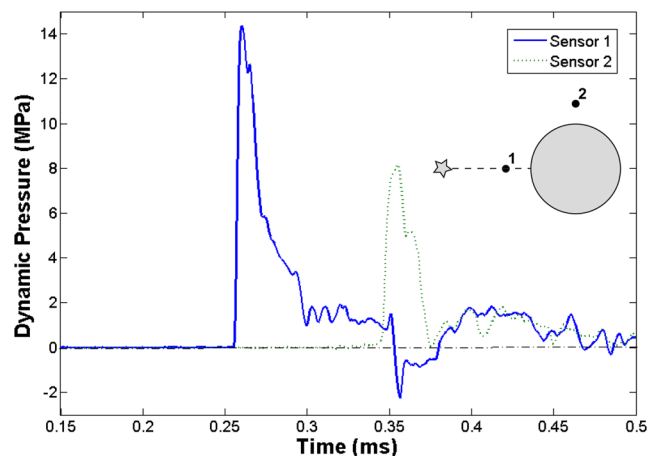


**Fig. 4** Initial shock wave measured at locations between the charge and specimen and directly above the specimen for the case of a 305 mm explosive standoff. The star in the image represents the location of the charge

pressures,  $P_r$  and  $P_t$  respectively, caused by an incident wave with pressure  $P_i$  are defined as:

$$P_r = R * P_i \quad P_t = (1 + R) * P_i \quad (1)$$

Where  $R$  is known as the reflection coefficient. The reflection coefficient for a normal incidence of a wave at a boundary is defined as [22]:

$$R = \frac{\rho_2 c_2 - \rho_1 c_1}{\rho_2 c_2 + \rho_1 c_1} \quad (2)$$

Where  $\rho$  is the material density,  $c$  is the sound speed of the material, and subscripts 1 and 2 refer to the material before and after the boundary, respectively. The density and sound speed for the water in this experiment are  $998 \text{ kg/m}^3$  and  $1488 \text{ m/s}$ , respectively. The through-thickness density and sound speed for carbon/epoxy composites has been reported as  $1611 \text{ kg/m}^3$  and  $3042 \text{ m/s}$ , respectively. For an acoustic wave traveling from water to the composite tube with normal incidence, the reflection coefficient was calculated as  $0.535$ . Simple acoustic theory can show [22], using Eq. 2, that upon encountering the surface of the tube, an incident wave with magnitude  $P_i$  creates a reflected wave with a magnitude  $0.535 P_i$ , and a transmitted wave with a magnitude of  $1.535 P_i$  maintaining the same compressive sign. The transmitted wave travels through the composite tube until it reaches the enclosed air volume. The reflection coefficient at this interface is approximately  $-1$ . This means that upon encountering this interface, all of the wave is reflected back into the composite wall with the same magnitude, but with opposite sign. This converts the pulse into a tensile wave which then travels back through the tube wall and into the surrounding fluid where it is observed by nearby sensors. Accounting for the reflection constant again at the composite-water interface calculated using Eq. 2, the magnitude of the tensile wave transmitted to the water

is  $0.821 P_i$ . This, coupled with attenuation in the various media, explains the reduced magnitude of the reflected tensile pulse observed in the pressure trace for sensors directly between the charge and the tube.

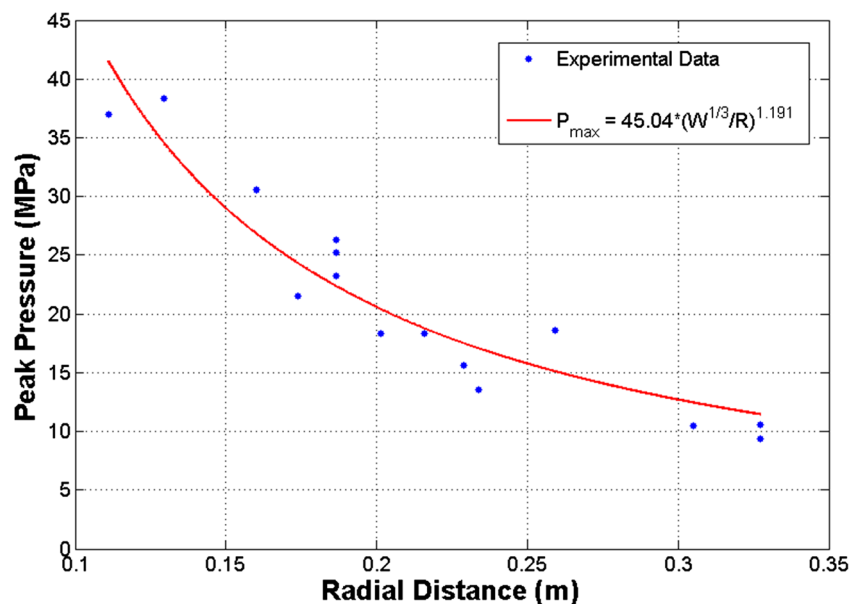
The important conclusion drawn from this analysis is that when a sealed composite tube is subjected to explosive loading, the pressure waves that travel through the walls of the structure are not solely compressive. If this tube is filled with a low impedance material such as air, tensile waves of significant magnitude will be caused in the tube wall by the impedance mismatch at the interior interface. This tensile loading has the potential to degrade the stability of the structure, as it may cause damage in the matrix material or at the fiber-matrix interface which are highly sensitive to out-of-plane tension [23].

### Identifying Features of the Pressure History

By its nature, the pressure fields generated in an underwater explosion in a closed tank are very noisy. Reflections from the initial shock wave and the “bubble pulse” are important features to identify, but superposition of these features can make that a challenge. To address this, acoustic wave theory coupled with an additional high-speed camera observing the explosive itself are used to distinguish these events.

The initial shock wave produced by the RP-85 detonator is characterized by recording peak pressures at several different standoff locations. The model proposed by Shin [24] is then fit to the data, to obtain a relationship by which the peak pressure could be predicted as a function of standoff distance. Experiments were conducted with just the explosive in the pressure vessel to characterize the loading pulse. The fit model is included in Fig. 5, and this was used to determine maximum incident pressures listed in Table 1.

**Fig. 5** Peak pressure of RP-85 as a function of standoff distance. The parameters for the fit curve are given in the plot for a charge of mass,  $W$ , in kilograms



Reflections of the initial shock are determined by assuming that pulse travels with acoustic wave speed, which in water is approximately 1500 m/s. At this velocity, the shock will travel to the tank boundaries and back to the sensors after 1.04–1.80 ms depending on the location of the charge. Using the same travel speed, a second reflection of that wave will arrive after 2.10–3.61 ms. Attenuation of the wave during travel will cause the reflections to be significantly lower magnitude and less sharp, and because the charge is not in the absolute center of the tank, the reflected wave will be recorded as a tight group of small peaks. For these reasons, the first and second reflections of the initial shock are identified as clusters of smaller spikes in the pressure located in the aforementioned time windows.

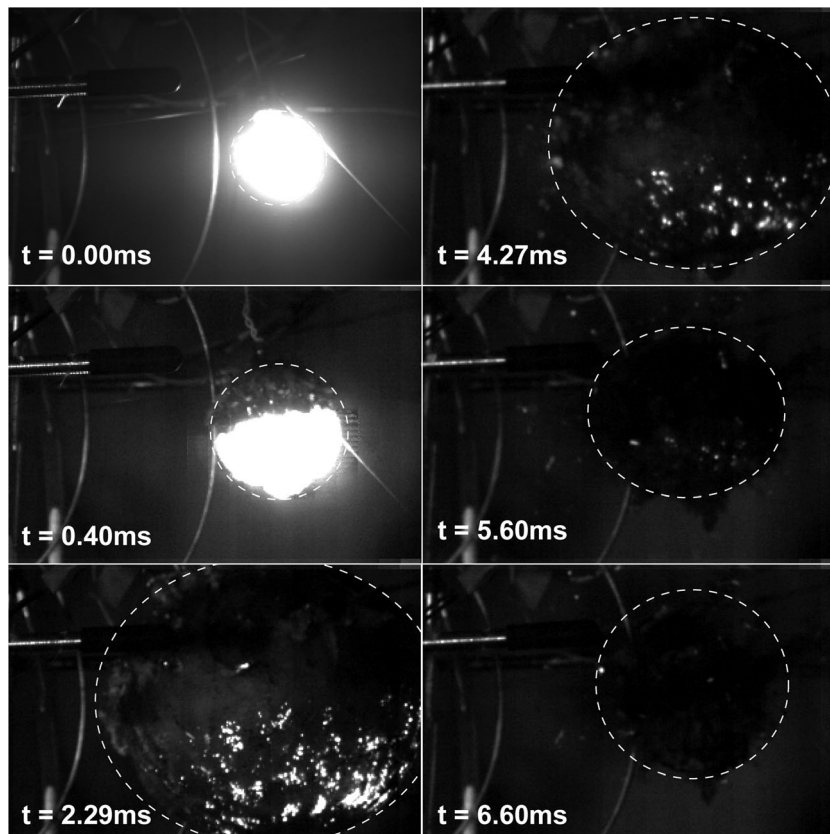
The additional high-speed camera is used to identify the bubble pulse. When an underwater explosive is detonated, the decomposed gases of the charge create an expanding superheated gas bubble. After reaching its maximum critical size, the surrounding hydrostatic pressure of water causes the bubble to collapse, and upon completion of this collapse, a relatively strong and fairly broad pressure pulse known as the “bubble pulse” is emitted [21]. The magnitude of the bubble pulse is typically much smaller than that of the initial shock wave, however due to its long duration, the impulse is of comparable strength. To identify the timing of this pulse, a typical growth of the bubble to its maximum size and

subsequent collapse is shown in Fig. 6. In all cases, the bubble grows to its maximum size at approximately 2.29 ms and collapses between 5.00 and 5.60 ms, so a broad pressure pulse found near this region in time is considered to be the bubble pulse.

### Near-Field Explosion (102mm Standoff)

The pressure history at the point on the specimen nearest to the charge for the 102mm standoff is plotted in Fig. 7, where the charge detonates at 0.00 ms (this time notation will be used throughout later in this article). In this case, the tube implodes shortly after experiencing the initial shock from the explosive. The initiation of the instability occurs at approximately 0.90 ms, well before the arrival of reflections from the tank wall, so it may be concluded that the initial shock wave alone possesses sufficient energy to trigger the collapse at this sub-critical static pressure. Wall contact occurs 5.00 ms after the initiation of the implosion, roughly consistent with results from natural implosion experiments. This implies that though the initiation mechanism of the collapse is different, the subsequent mechanics of the collapse are the same as for a natural implosion. In this case, no implosion pulse is detectable in the pressure history following wall contact. This is due to the noisy nature of the pressure signal at this time caused by the

**Fig. 6** High-speed images of the growth and collapse of the gas bubble, the boundary of which is indicated by a dashed white line. Here the bubble reached maximum size at 2.29 ms after detonation and collapsed at 5.60 ms



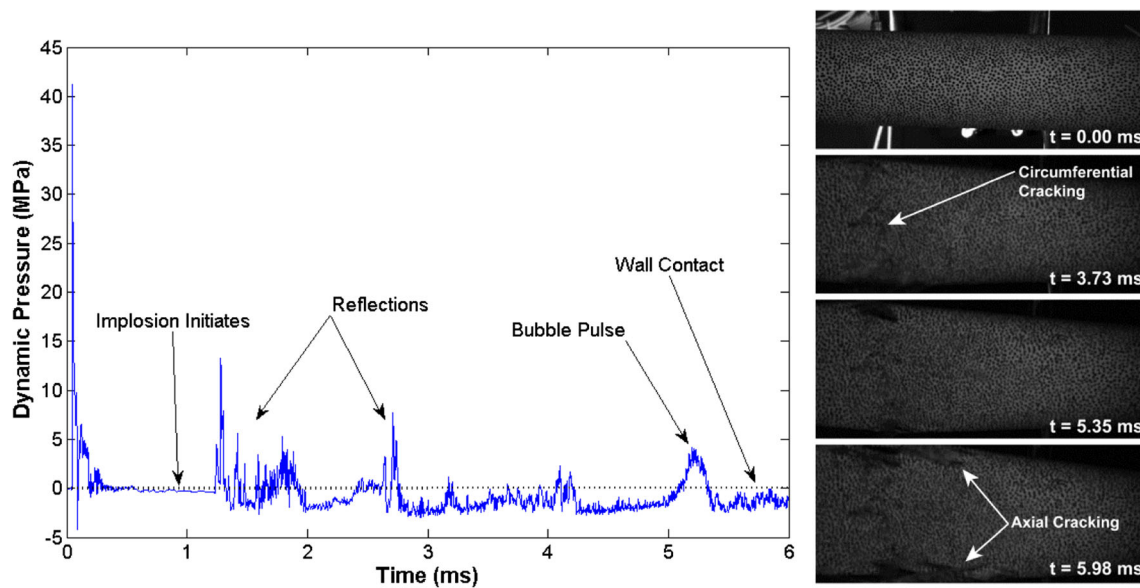


**Fig. 7** Pressure history (*left*) and high-speed images (*right*) for explosive experiments with 102mm standoff

superposition of reflections of the initial shock and bubble pulses from the tank walls.

Though the time to collapse is consistent with the natural implosion, a unique feature of this case is the initiation of observable damage prior to wall contact. The high-speed images in Fig. 7 show that a large degree of circumferential cracking occurs 2.21 ms prior to wall-contact, located at the midspan of the tube. These cracks are seen in post-mortem images (Fig. 8) to run parallel to reinforcing fibers, implying that they occur in the resin-rich regions between fibers. The center of the tube experiences the most severe loading, as it is the closest to the charge. The cause for this early damage is the particular wave interaction discussed in Section 3.2. The resulting tensile loading within the tube wall is enough to cause inter-fibrillar as well as matrix cracking, as seen in the high-speed images. This cracking significantly degrades the structural stability, and is a contributing factor in the damage initiation eventually leading to the implosion.

Post-mortem images in Fig. 8 show very extensive damage to the tubes, mainly in the form of through-thickness axial cracks (B) and circumferential cracks (A) localized about the midspan of the tube. The axial cracks in these tubes completely separate sections of the tube, and several frayed and pulled-out fibers are seen on the faces of the cracks. This shows that these cracks form in a very high energy event, enough to fracture both matrix and fiber in all seven plies and cause the pull-out of adjacent fibers. The axial cracking for this case is more extensive than all other cases, including that of natural implosion. Pegg [9] demonstrated that hydrostatic pressure combined with strong impulse loads result in more severe deformations, which is the reason for the extent of damage. In comparison, the circumferential cracks at the midspan are much less severe. These cracks do not penetrate completely

through the tube wall, do not travel very far from the tube midspan, and cause no fiber pull-out.

### Mid-Field Explosion (203mm Standoff)

The pressure history at the point on the specimen nearest to the charge for the 203mm standoff is plotted in Fig. 9. Implosion again occurs in this case, though it is much later in the time than the 102mm standoff case, initiating 6.53 ms after the detonation of the charge. This delayed collapse shows that

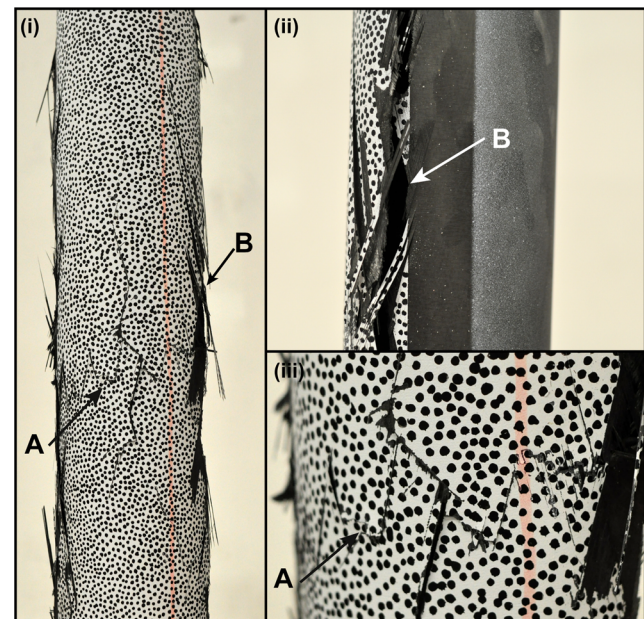


**Fig. 8** Post-mortem images showing the full-length (i), a side-view (ii), and a zoomed image of the tube center for 102mm explosive standoff. These images display circumferential cracking (a) and dramatic, through-thickness axial cracking (b)

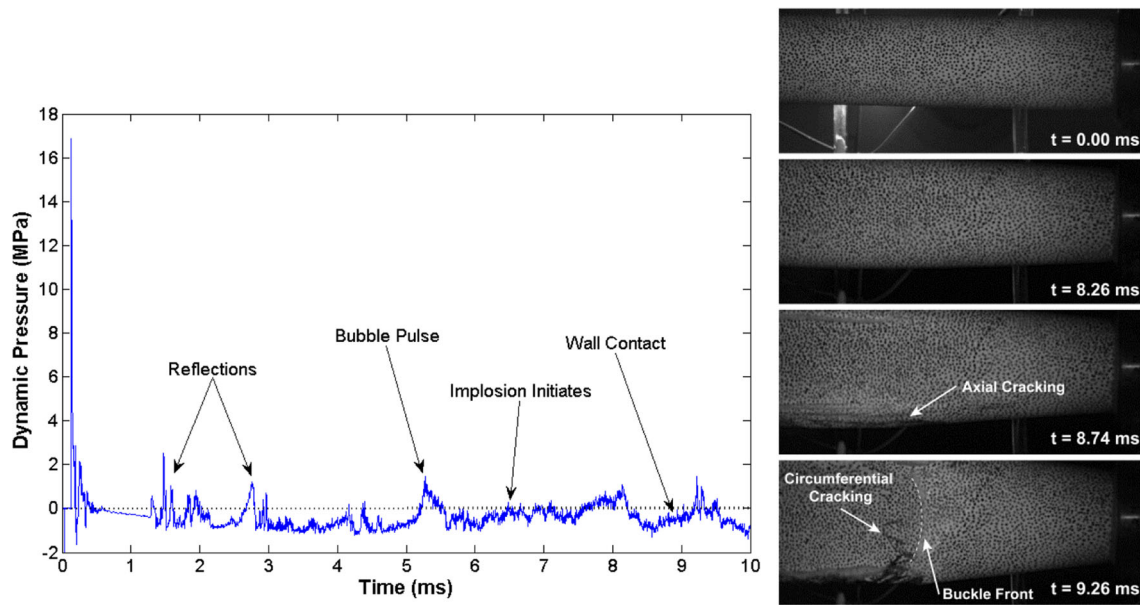


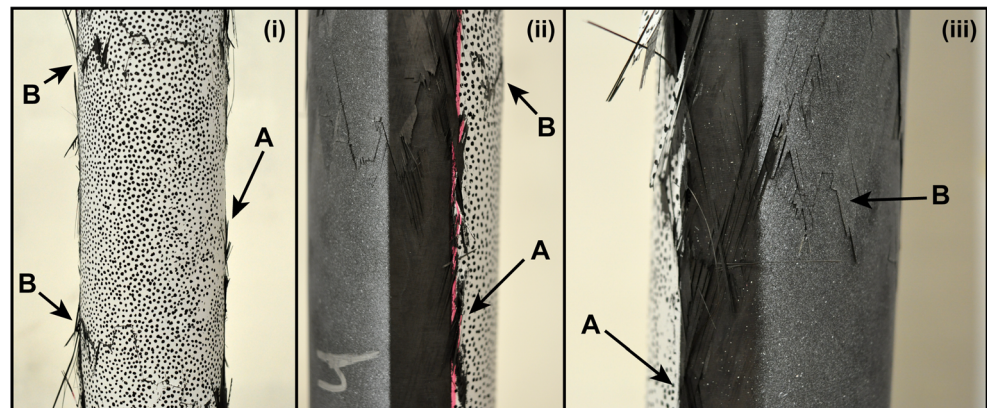
**Fig. 9** Pressure history (*left*) and high-speed images (*right*) for explosive experiments with 203mm standoff

neither the initial shock wave nor the reflections of that shock from the tank walls are sufficient to cause the collapse at this charge distance. The instability is triggered after the first bubble pulse showing that for this standoff distance, the bubble pulse is the cause of the implosion. The tube continues to collapse until wall contact is made 2.43 ms after initiation, which is significantly shorter than the collapse time of the natural implosion (4.7 ms). The reason behind this reduction in collapse time, as well as the reason for the timing of the collapse, is related to the wave interaction discussed in Section 3.2. Each feature of the pressure trace that encounters the specimen - the initial shock, reflections, and the bubble pulse - results in tensile loading within the tube wall. Unlike the previous case, the loading is not severe enough to exceed the tensile strength of the matrix. Examining high-speed images in Fig. 9, no visible cracking occurs from the impact of the shock or the subsequent reflections and bubble pulse. However, damage may still occur within the material. This repeated loading can degrade the fiber/matrix interface, cause

and/or propagate delaminations, and grow any pre-existing defects where stress concentrations may occur. The net result is that at each loading event, damage will accumulate in the material, which will reduce its stiffness and structural integrity. In this case, damage accumulates enough in the first 5.00 ms of the pressure history that the energy supplied by the bubble pulse is sufficient to initiate the instability. As is the case with 102 mm standoff distance, the implosion pulse is not reliably distinguished for these experiments due to the noisy nature of the pressure field at the time which it occurs.

Post-mortem images (Fig. 10) again show large amounts of damage, including through-thickness axial cracks (A) and circumferential cracks (B) offset from the midspan. Though the axial cracks do penetrate completely through the thickness of the tube wall, they are significantly less severe than for the previous case. Fiber pull-out is observed in the vicinity of these cracks, however there is no separation of the tube walls, and the structure maintains a large portion of its integrity. The circumferential cracks appear similar to those seen in the

**Fig. 10** Post-mortem images of the front (i) and side faces (ii & iii) for 203mm explosive standoff, showing axial cracking (a) and multiple instances of circumferential cracking (b)





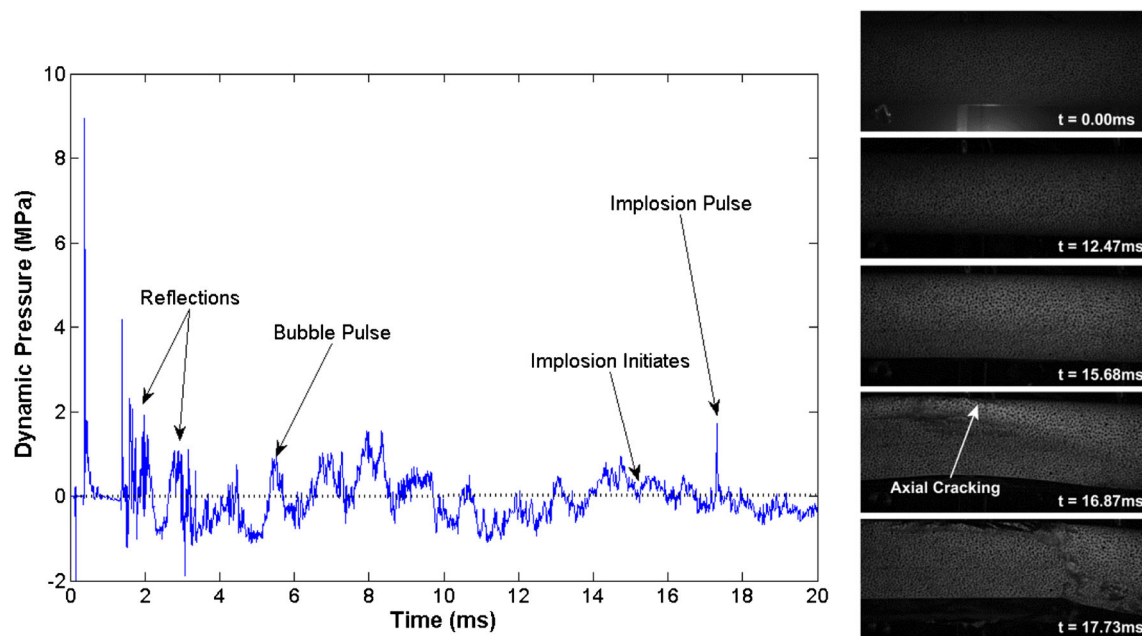


**Fig. 11** Pressure history (*left*) and high-speed images (*right*) for explosive experiments with 305mm standoff

previous case, however their location and cause are quite different. These cracks are seen to appear only after wall contact has made and the flattening of the tube has propagated past the point where the cracks emerge. This shows that these cracks are not a result of the incident shock, but rather due to the large deformations resulting from the buckle propagation.

#### Far-Field Explosion (305mm Standoff)

The pressure history at the point on the specimen nearest to the charge for the 305mm standoff is plotted in Fig. 11. Similar to the previous two cases, these tubes implode in a mode 2 shape, however they collapse very late in the event, initiating 15.26 ms after the detonation of the charge. This is long after both the initial shock and the first bubble pulse, showing that neither of these events trigger the collapse on their own. Wall contact occurs at 1.83 ms following the initiation of the implosion, even shorter than for the 203mm standoff case. Like the 203 mm standoff case, the cause for the delayed collapse as well as the duration of the collapse is due to the accumulation of damage caused by each successive loading event in the pressure history. This damage continually degrades the structural stiffness, until the vibrations caused by the impulse coupled with hydrostatic pressure can drive the implosion. The development of visible damage as seen in the high-speed images is less severe than for this case as no circumferential cracking appears at any time.

In this case, the pressure field has settled enough that an implosion pulse is clearly distinguished. Wall contact occurs at 17.09, and 0.21 ms later a sharp high magnitude pressure spike is recorded with strength of 1.67MPa. The magnitude and timing of this pulse is consistent with that seen in natural

implosion experiments, giving additional evidence that this is in fact an implosion pulse.

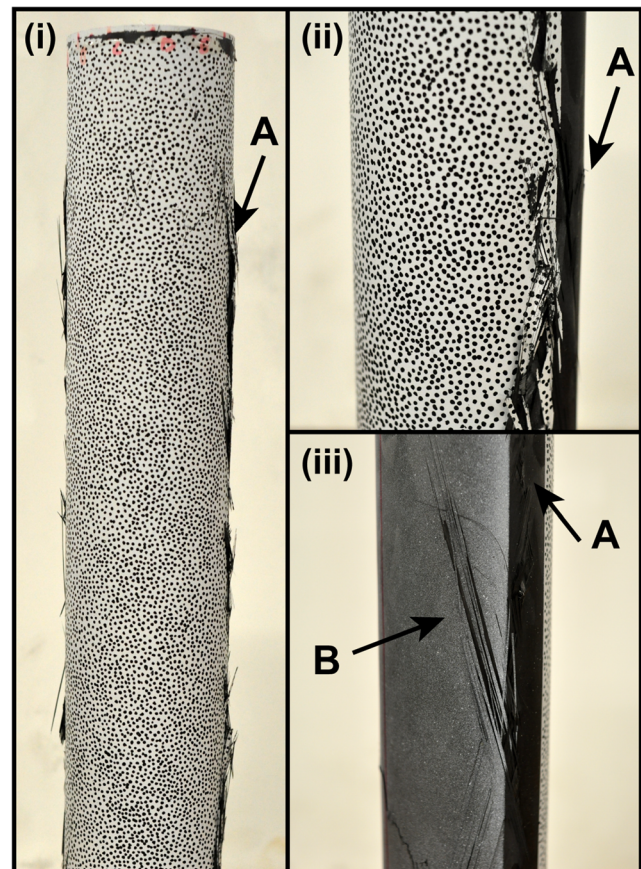


**Fig. 12** Post-mortem images of the front (i), side (ii), and back (iii) faces for 305mm explosive standoff, showing axial cracking (**a**) and adjacent outer ply cracks (**b**)

Post-mortem images of these specimens (Fig. 12) show the least damage of all cases, mainly in the form of through-thickness axial cracks (A). Referring back to the high-speed images in Fig. 11, these cracks appear shortly before wall contact is made, implying that they are a result of extreme bending strains at that time. Some fiber pull-out is seen near these cracks as well as interfibrillar cracking in the outer ply, parallel to the 15° fiber angle of that layer (B). The net damage in the structure is still far less extensive than that found in the previous two cases, due to the greatly reduced intensity of the incident shock (see Table 1).

### DIC Analysis of Initial Shock Response

From previous work, it is known that prior to a dynamic collapse, hollow cylinders experience some degree of quasi-static ovaling due to hydrostatic pressure [7, 8, 18]. For a natural implosion, a maximum pre-buckling radial deformation of  $-1.57\text{mm}$  is measured prior to the dynamic collapse. At 80% of the critical collapse pressure, the pre-buckling reaches only  $-0.56\text{mm}$ , showing that a significant perturbation of more than 1mm is required to reach a region of instability.

DIC is also used to compare the initial response of the tube to the shock loading. Figure 13 shows contours of velocity magnitude across half of the length of the tube over time. The first observation that can be made is the uniformity of loading across the length of the structure. At the close standoff, the initial response of the structure is very localized near the center of the tube. For higher standoffs, the response is more uniform across the length of the specimen. As standoff distance is increased, the front of the pressure wave becomes increasingly planar due to geometric spreading, and will load a greater area upon initial impact. The magnitudes of the initial velocities are also quite different. For the 102mm, 203mm, and 305mm standoffs, tubes show a maximum initial velocity of 13m/s, 5.7m/s, and 4.5 m/s, respectively. This reduction is expected, since the peak pressure of the initial shock wave will decay as  $\frac{1}{R_e}$ , where  $R_e$  is the distance from the explosive. The difference in uniformity of the loading across the length of the tube, coupled with the difference in peak velocity greatly affects the dynamic response of the structure.

More important in this Figure is the visible difference in modal response of the structure to each loading case. For the farthest standoff distance, the tube appears to vibrate with a

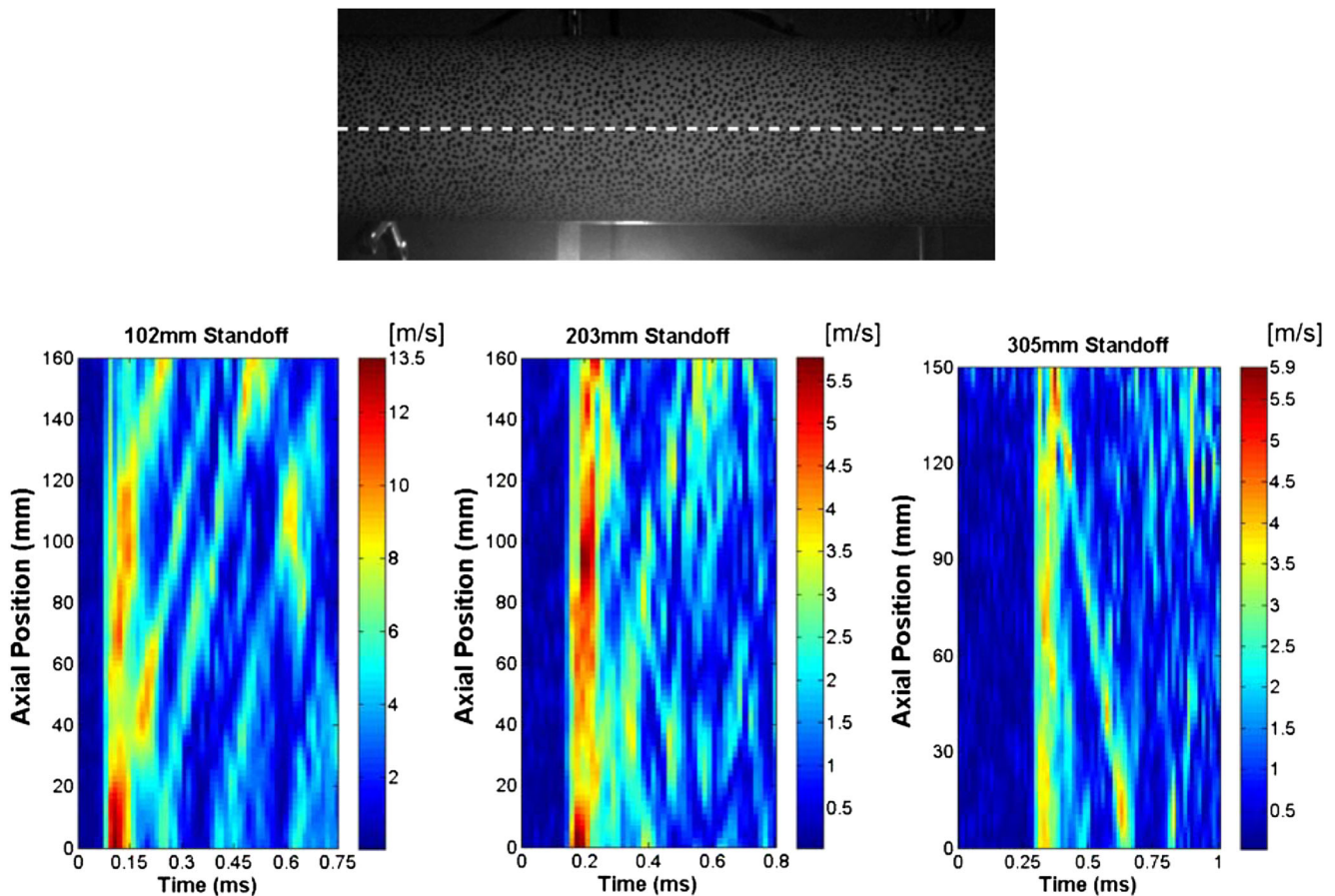


**Fig. 13** Velocity contours for half of the length of each specimen after impact of the initial shock. The top image indicated the location of DIC data extraction with a dashed white line. The zero point on the y-axis indicates the center of the tube, and color represents velocity magnitude in meters/second

single axial lobe. After the initial impact of the shock, a single region of elevated velocity is seen to travel along the length, implying a single lobe of deformation. For the closest standoff, the response following the arrival of the shock is quite different. Here, multiple regions of high velocity are seen propagating axially along the tube at the same instant. This implies that at closest standoff, the initial localized shock wave excites higher-order axial modes in the structure, which is why the wave is able to initiate the instability. In the absence of damage, impulse-initiated buckling occurs due to the vibrations of the structure due to the applied shock [2]. The closest standoff excites higher-order vibrations with relatively high velocities, which provides a sufficient perturbation to trigger the collapse. In addition, previous research has shown that short pulse durations characteristic of explosive loads necessitate very high peak pressures to initiate an implosion [2]. For these reasons, neither of the larger standoffs are capable of causing a collapse from the initial shock alone, but rely on subsequent growth of damage.

## Conclusions

The explosive-initiated implosion of carbon/epoxy composite tubes is studied for varying incident shock wave strengths. High-speed photography, DIC measurements, and dynamic pressure sensors are used to characterize the mechanisms of collapse for each case studied. The completion of this study has resulted in the following conclusions:

- A composite tube may implode at pressures 20% below the critical static pressure if it experiences impulsive loading from a nearby explosive.
- Explosive initiated implosions of composite tubes may occur due to: (i) the initial shock, (ii) the bubble pulse, or (iii) long after both of these features due to the accumulation of damage.
- The failure of composite tubes under these shock wave loading is fundamentally different from homogenous materials. It is largely governed by the damage created within the material due to high magnitude tensile waves reflected from the inner solid/air boundary.
- The implosion pulse generated from the collapse of the tubes is typically obscured in the pressure history, however in the case of a long delayed collapse, this pulse may be distinguished and is consistent with that generated in a natural implosion.
- The DIC technique can be used to extract the initial vibration response of the structure following loading, and shows that higher order modes are excited for closer standoffs distances leading to the dynamic collapse.

**Acknowledgments** The authors would like to acknowledge the Office of Naval Research and Dr. Yapa D.S. Rajapakse for providing financial support to conduct this research under Grant No. N00014-10-1-0662.

## References

1. Mouritz AP, Gellert E, Burchill P, Challis K (2001) Review of advanced composite structures for naval ships and submarines. *Compos Struct* 53(1):21–42
2. Lindberg HE, Florence AL (1987) *Dynamic pulse buckling: theory and experiment*. M. Nijhoff, Dordrecht
3. Moon CJ, In-Hoon K, Bae-Hyeon C, Jin-Hwe K, Choi JH (2010) Buckling of filament-wound composite tubes subjected to hydrostatic pressure for underwater vehicle applications. *Compos Struct* 92(9):2241–251
4. Ross CTF, Little APF, Haidar Y, Waheeb AA (2009) Buckling of carbon/glass composite tubes under uniform external hydrostatic pressure. *Strain* 47:156–174
5. Smith PT, Ross CTF, Little APF (2009) Collapse of composite tubes under uniform external hydrostatic pressure. *J Phys: Conf Ser* 181:156–157
6. Hur SH, Son HJ, Kweon JH, Choi JH (2008) Postbuckling of composite tubes under external hydrostatic pressure. *Compos Struct* 86(1–3):114–24
7. Pinto M, Gupta S, Shukla A (2014) Study of implosion of carbon/epoxy composite hollow cylinders using 3-D digital image correlation. *Compos Struct* 119:272–286
8. Pinto M, Gupta S, Shukla A (2015) Hydrostatic implosion of GFRP composite tubes studied by digital image correlation. *J Press Vess Technol* 137(5):051302
9. Pegg NG (1994) Effects of impulse duration and combined impulse-hydrostatic pressure on buckling stability of cylindrical structures. *J Ship Res* 38(2):164–71
10. Tanov R, Tabiei A, Simitzes G (1999) Effect of static preloading on the dynamic buckling of laminated cylinders under sudden pressure. *Mech Adv Mater Struct* 6(3):195–206
11. Krueger SR (2006) Simulation of cylinder implosion initiated by an underwater explosion. Naval Postgraduate School, Monterey
12. Hoo Fatt MS, Pothula SG (2010) Dynamic pulse buckling of composite shells subjected to external blast. *Compos Struct* 92(7):1716–727
13. Brett J, Yiannakopoulos G (2008) A study of explosive effects in close proximity to a submerged cylinder. *Int J Impact Eng* 35(4):206–25
14. Hung CF, Lin BJ, Hwang-Fuu JJ, Hsu PY (2009) Dynamic response of cylindrical shell structures subjected to underwater explosion. *Ocean Eng* 36(8):564–77
15. Ikeda, CM (2012) Fluid–structure Interactions Implosions of Shell Structures and Wave Impact on a Flat Plate. Thesis. University of Maryland, College Park
16. Arora H, Hooper PA, Dear JP (2012) The effects of Air and underwater blast on composite sandwich panels and tubular laminate structures. *Exp Mech* 52:59–81
17. Sutton MA, Orteu JJ, Schreier HW (2009) *Image correlation for shape, motion and deformation measurements: basic concepts, theory and applications*. Springer, New York
18. Gupta S, Parameswaran V, Sutton MA, Shukla A (2014) A study of underwater implosion using digital image correlation. *Proc R Soc A* 470(2172):20140576

19. Turner SE, Ambrico JM (2012) Underwater implosion of cylindrical metal tubes. *J Appl Mech* 80(1):1–11
20. Ikeda CM, Wilkerling J, Duncan JH (2013) The implosion of cylindrical shell structures in a high-pressure water environment. *Proc R Soc A: Math Phys Eng Sci* 469:2160
21. Cole RH (1948) *Underwater explosions*. Princeton University, Princeton
22. Kinsler LE, Frey AR (1962) *Fundamentals of acoustics*. Wiley, New York
23. Sridharan S (2008) *Delamination behaviour of composites*. Woodhead, Cambridge
24. Shin YS (2004) Ship shock modeling and simulation for far-field underwater explosion. *Comput Struct* 82(23–26):2211–219